CHEMISTRY OF MATERIALS

Article

pubs.acs.org/cm

Conformation-Insensitive Ambipolar Charge Transport in a Diketopyrrolopyrrole-Based Co-polymer Containing Acetylene Linkages

Hui-Jun Yun,[‡,∇] Hyun Ho Choi,[†,∇] Soon-Ki Kwon,*[,‡] Yun-Hi Kim,*[,§] and Kilwon Cho*[,†]

[†]Department of Chemical Engineering, Pohang University of Science and Technology (POSTECH) and Center for Advanced Soft Electronics (CASE), Pohang 790-784, Korea

[‡]School of Materials Science and Engineering, Research Institute for Green Energy Convergence Technology (REGET), Gyeongsang National University, Jinju 660-701, Korea

[§]Department of Chemistry, Gyeongsang National University and Research Institute of Nature Science (RINS), Jinju 660-701, Korea

Supporting Information

ABSTRACT: A new donor−acceptor organic semiconducting co-polymer (PDPP-TAT) containing acetylene linkages based on dithienyl-diketopyrrolopyrrole (tDPP) has been synthesized and compared with a tDPP-based co-polymer (PDPP-TVT) containing vinylene linkages. The *sp*-hybridized carbons in the acetylene linkages result in favorable overlap of the electron wave functions of the tDPP units along the main chain. Further, the π-conjugation of PDPP-TAT was found to be highly insensitive to the chain conformation, in contrast to that of PDPP-TVT. As a result, PDPP-TAT provides favorable charge transport for electrons as well as holes, and enables facile charge transport in amorphous and tie-molecular regions connecting its crystalline domains. PDPP-TAT exhibits ambipolar characteristics with a high electron/hole mobility ratio (μ_e/μ_h) of ∼0.3 in field-effect transistors, whereas PDPP-TVT exhibits unipolar characteristics with a μ_e/μ_h value that is a factor of 30 lower. Our results demonstrate that the conformation sensitivity of charge transport is a vital factor in the electrical performances of actual organic transistor devices.

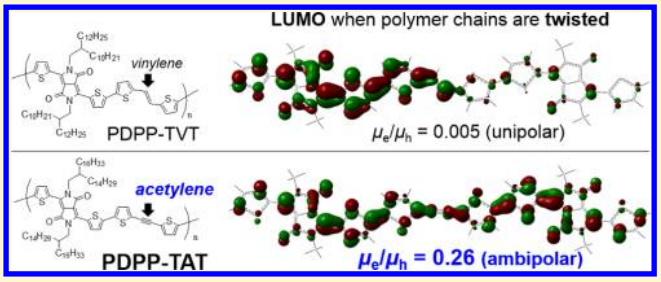

INTRODUCTION

Ambipolar organic field-effect transistors (ambipolar FETs) based on both *p*-type and *n*-type channels have recently attracted great interest, because of the simplicity of their circuit design and fabrication.[1−6] For example, a complementary metal-oxide-semiconductor (CMOS)-like inverter can easily be constructed by combining two identical ambipolar FETs. Several types of high-performance ambipolar FETs have been developed.[7−15] Most ambipolar FETs based on a dual-nature organic semiconductor are superior to unipolar component systems (i.e., to bilayers or bulk-heterojunction blends), in terms of the aforementioned requirements.

Recent research into dual-nature organic semiconductors has developed low-bandgap co-polymers based on alternating conjugated donor−acceptor (D-A) dyads as the building blocks of the polymer backbones, which are expected to exhibit ambipolarity and highly π-extended conjugation.[16−18] The intramolecular charge transfer within these D−A systems, namely, the push−pull effect, can be readily manipulated to yield high charge carrier mobilities. Moreover, the low bandgaps of these co-polymers mean that the charge injection from electrodes to their HOMO and LUMO levels is facile, because of the low-energy offsets between the metals' Fermi levels and the frontier energy levels (i.e., the HOMO and LUMO) of the co-polymers. The use of the diketopyrrolopyrrole (DPP) moiety as an acceptor unit in such co-polymers is of particular interest, because the thiophene-coupled DPP moiety (tDPP) has been reported to have remarkable aggregation properties.[18−22] The favorable intramolecular sulfur−oxygen interactions of the tDPP moiety mean that it is nearly co-planar, which results in high planarity with low dihedral angles between DPP and the adjacent thiophene units. This planarity is expected to allow long conjugation length along the intrachain and facilitate strong intermolecular $\pi-\pi$ interaction, which is associated with good charge transport properties.

Janssen and Li groups synthesized the homopolymer of tDPP and found it to exhibit ambipolar FET properties.[23,24] However, the reported FET mobilities for both hole and electron were quite low. In attempts to improve the properties of the tDPP homopolymer, additional donor units composed of thiophene or selenophene have been introduced between the tDPP components. The DPP acceptor unit typically has branched alkyl side chains which hinder close intermolecular

Received: April 23, 2014
Revised: June 18, 2014

   dx.doi.org/10.1021/cm5014703 | *Chem. Mater.* XXXX, XXX, XXX−XXX

$\pi-\pi$ stacking at thiophene sites.[25,26] By inserting additional thiophene (T) or selenophene (S) units, the resultant donor components act as spacers that permit closer intermolecular $\pi-\pi$ stacking. The $\pi-\pi$ distance of the tDPP homopolymer is 3.75−3.82 Å,[23,24] whereas co-polymers with inserted thiophene, bithiophene, or terthiophene units (with monomer structures T[tDPP], TT[tDPP], or TTT[tDPP], respectively) have closer $\pi-\pi$ distances in the range of 3.65−3.75 Å.[27−29] Thus, facilitated intermolecular charge transport can be obtained in thin films of tDPP-based co-polymers.

However, this approach can hinder intrachain electron transport and, thus, eliminate the ambipolarity. Intrachain overlap of the electron wave functions of the tDPP acceptor units is required for ambipolarity, but the long donor components separate these units and localize the electrons. For example, the T[tDPP]- and S[tDPP]-structured co-polymers contain short donors (T denotes thiophene, S denotes selenophene) and exhibit ambipolar characteristics in FET devices,[27,30−32] whereas TT[tDPP]-, SS[tDPP]-, TTT-[tDPP]-, and SSS[tDPP]-structured co-polymers contain long donors and exhibit hole-accumulated unipolar characteristics.[28,29,33−36] Recently, our group reported record FET mobilities in devices using the TT[tDPP]- and SS[tDPP]-structured co-polymers: tDPP−thiophene−vinylene−thiophene (PDPP-TVT) and tDPP−selenophene−vinylene−selenophene (PDPP-SVS), respectively.[25,34] The introduction of TVT or SVS as donor units with rigid vinylene (V) linkages can extend the polymer coplanarity, and results in not only a long intrachain π-conjugation length but also in enhanced intermolecular $\pi-\pi$ stacking. However, as is consistent with previous studies of TT[tDPP]- and SS[tDPP]-structured co-polymers, the long distance between the acceptors in the T═T[tDPP] and S═S[tDPP] structures prevents electron transport and results in unipolar charge transport.

Here, we propose a method for inducing ambipolarity in tDPP-based co-polymers with a long donor system. A triple-bonded acetylene (A) linkage is inserted into the long donor component of the TT[tDPP] system to produce a final architecture of T≡T[tDPP] (PDPP-TAT). The acetylene linkage is highly rigid and, similar to the vinylene linkage, extends the π-electrons. We found that the acetylene linkage acts as a bridge in the delocalization of the electrons at tDPP sites, because of the electron acceptor characteristics of its *sp*-hybridized carbons. The rigid acetylene linkages produce fluent π-electron densities with cylinder-like forms and, therefore, are also expected to preserve the co-planarity of the thiophene moieties, as well as enhance the intermolecular interactions. Furthermore, the π-conjugation of the synthesized polymer is highly insensitive to the chain conformation, which results in facile charge transport in the amorphous regions connecting its crystalline domains. In contrast to the T−T[tDPP]-, S−S[tDPP]-, T═T[tDPP]-, and S═S[tDPP]-structured co-polymers such as PDPP-TT, PDPP-SS, PDPP-TVT, and PDPP-SVS, the T≡T[tDPP]-structured PDPP-TAT exhibits ambipolarity in FET devices, a 10^1-10^3 times higher electron mobility of 0.38 $cm^2\ V^{-1}\ s^{-1}$, and an electron/hole mobility ratio of ∼0.26.

EXPERIMENTAL SECTION

Materials. All reactions were carried out in a nitrogen atmosphere, using the usual Schlenk techniques. All chemical reagents were purchased from Aldrich and used as received. 1,2-Di(thiophen-2-yl)ethyne, and 3,6-dithiophen-2-yl-2,5-dihydropyrrolo[3,4-*c*]pyrrole-1,4-dione were prepared according to literature procedures.[37] All solvents were further purified prior to use.

Synthesis of Poly(2,5-bis(2-tetradecyloctadecyl)-3-(thiophen-2-yl)-6-(5′-(thiophen-2-ylethynyl)-2,2′-bithiophen-5-yl)-pyrrolo[3,4-*c*]pyrrole-1,4(2H,5H)-dione) (PDPP-TAT). The polymer was prepared using a palladium-catalyzed Stille coupling reaction. 3,6-bis(5-bromothiophen-2-yl)-2,5-bis(2-tetradecyloctadecyl)pyrrolo-[3,4-*c*]pyrrole-1,4(2H,5H)-dione (0.30 g, 0.221 mmol) and other1,2-bis(5-(trimethylstannyl)thiophen-2-yl)ethyne (114.14 mg, 0.221 mmol) were dissolved in dry toluene (8.5 mL) and dimethyl formamide (DMF) (1.5 mL). The monomer synthesis is described in Supporting Information. After degassing under nitrogen for 60 min, tetrakis(triphenylphosphine)palladium(0) $Pd(pph_3)_4$ (20 mg) was added to the mixture and was stirred for 12 h at 90 °C. 2-Bromothiophene and tributyl(thiophen-2-yl)stannane were injected sequentially into the reaction mixture for end-capping, and the solution was stirred for 6 h after each addition. The polymer was precipitated in methanol. The crude polymer was collected by filtration and purified by Soxhlet extraction with methanol, acetone, hexane, toluene, and chloroform, successively. The PDPP-TAT was obtained by precipitation in methanol. Yield: 63%. (Number-average mass (M_n) = 73 000, weight-average mass (M_w) = 96 000, PDI = 1.31). ^{1}H NMR ($CDCl_3$, 500 MHz), δ (ppm): δ 8.75−7.79 (br, 4H), 7.65−7.22 (br, 2H), 6.65−6.40 (br, 2H), 4.53−4.12 (br, 4 H), 2.20−2.11 (br, 2 H), 1.78−1.00 (br, 112 H), 0.92−0.85 (br, 12H).

Characterization. ^{1}H NMR and ^{13}C NMR spectra were recorded with a Bruker Model Avance-300 spectrometer. The thermal analysis was performed on a TA Instruments Model TGA 2100 thermogravimetric analyzer in a nitrogen atmosphere at a rate of 10 °C/min. Differential scanning calorimetry (DSC) was conducted under nitrogen on a TA Instruments Model 2100 DSC system. The sample was heated at a rate of 10 °C/min, from 30 °C to 300 °C. UV−vis absorption spectra were measured by a Model UV-1650PC spectrophotometer. Molecular weights and polydispersities of the co-polymers were determined by gel permeation chromatography (GPC) analysis with polystyrene standard calibration (Waters Model M515). Cyclic voltammetry (CV) was performed on an EG and G Parc Model 273 Å potentiostat/galvanostat system with a three-electrode cell in a solution of 0.1 M tetrabutylammonium perchlorate (Bu_4NClO_4) in acetonitrile at a scan rate of 50 mV/s. A Pt wire was used as the counter electrode, and an $Ag/AgNO_3$ (0.1 M) electrode was used as the reference electrode. The morphologies and thickness of the thin films were analyzed with a Veeco NanoScope IIIa atomic force microscope. The thickness of the thin films are 50−80 nm. Their molecular ordering was analyzed using two-dimensional grazing-incidence X-ray diffraction (2D-GIXD) at the 3C Beamline of Pohang Acceleration Laboratory. Density fiunctional theory (DFT) calculations were performed using the Gaussian 09 package with the nonlocal hybrid Becke three-parameter Lee−Yang−Parr (B3LYP) function and the 6-31G basis set to elucidate the HOMO and LUMO levels after optimizing the geometry of PDPP-TAT, using the same method. All devices were characterized using a Keithley Model 2636A SourceMeter under vacuum (10^{-3} Torr).

Device Fabrication. All procedures were performed in N_2-purged glovebox. A highly doped *n*-Si wafer with a 300-nm-thick thermally grown SiO_2 layer was used as a substrate. A 40−45-nm-thick Cytop (Asahi Glass) was spin-coated onto it; hence, Cytop/SiO_2 double layers work as the gate dielectric, whose capacitance is 8.1 nF cm^{-2} at 1 MHz. In order to form well-coated PDPP-TVT or PDPP-TAT thin films on Cytop, we accelerated solvent evaporation (chloroform) during the spin coating. At first, the solutions and substrates were preheated to 55 and 70 °C, respectively, on a hot plate. Next, the substrates were transferred to a spin coating stage. They were finally cooled to 55−60 °C due to heat transfer. Next, a warm chloroform solution (10 mg mL^{-1} at 55 °C) containing PDPP-TVT or PDPP-TAT was deposited onto the warm substrate dropwise and spin-coated. The spin speed was 4000−5000 rpm. Note that the spinning was performed immediately after the solution was deposited dropwise onto the substrate. The time interval between solution deposition and spinning steps was found to result in a significant spatial variance of

dx.doi.org/10.1021/cm5014703 | *Chem. Mater.* XXXX, XXX, XXX−XXX

Scheme 1. Synthetic Routes for PDPP-TVT and PDPP-TAT[a]

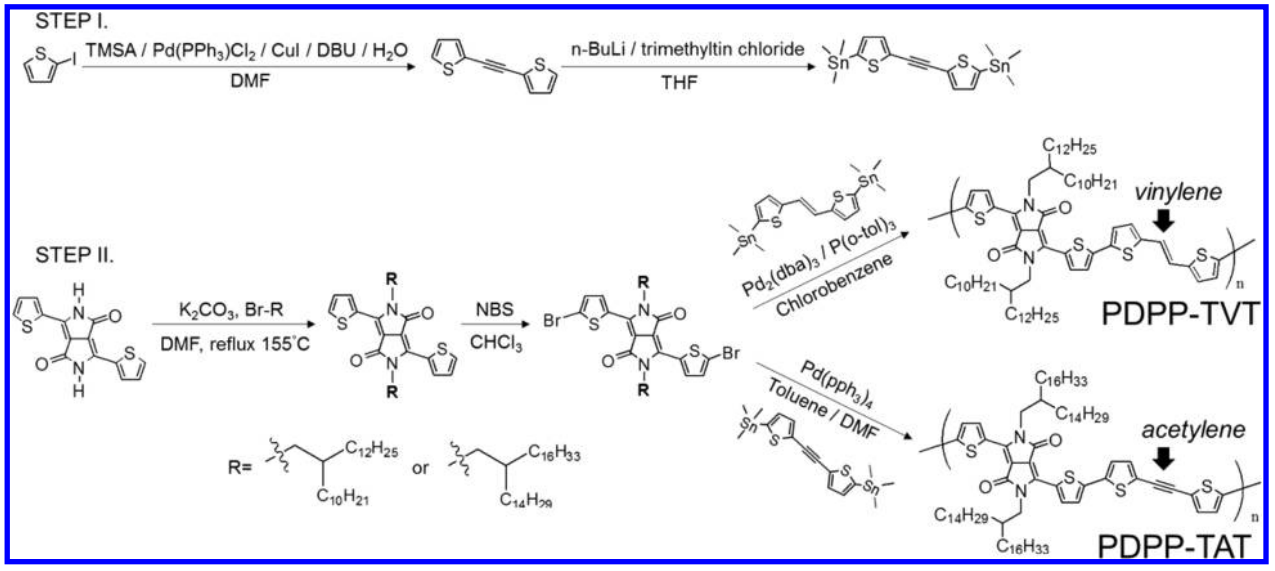

[a]The synthetic route for PDPP-TVT is that of ref 28. All the details of the synthesis of PDPP-TAT can be found in the Experimental Section and the Supporting Information.

FET performance. The films were thermally annealed at 100, 150, 200, or 250 °C for 15 min in N_2 environment. They were not dewetted and maintained their homogeneity after thermal annealing. The thermally deposited 50-nm-thick Al layer was used as source-drain electrodes; the channel width (W) and length (L) were 1000 μm and 150 μm, respectively.

RESULTS AND DISCUSSION

In this paper, we synthesized PDPP-TVT as well as PDPP-TAT, and then compared their physical, chemical, and electrical properties. PDPP-TAT (Scheme 1) was synthesized by performing the palladium-catalyzed Stille coupling reaction between 1,2-bis(5-(trimethylstannyl)thiophen-2-yl)ethyne and 3,6-bis(5-bromothiophen-2-yl)-2,5-bis(2-tetradecyloctadecyl)-pyrrolo[3,4-*c*]pyrrole-1,4(2H,5H)-dione with long branched C32 alkyl groups. The syntheses of the monomers and polymers are described in detail in the Supporting Information and the Experimental Section. PDPP-TVT (Scheme 1) was prepared according to an established procedure.[28] After each polymer had been purified by performing successive Soxhlet extractions with acetone, methanol, and hexane to remove the metal catalyst, it was dissolved in chloroform and precipitated into methanol. The structures of the monomers and polymers related to PDPP-TAT were confirmed with ^{1}H NMR and ^{13}C-NMR (see the Supporting Information). The number-average molecular weight (M_n) of PDPP-TAT was found to be 73.0 kDa with a polydispersity index (PDI) of 1.31. The M_n of PDPP-TVT was determined to be 82.1 kDa with a PDI of 2.3. Although PDPP-TAT has high rigidity, which is due to the introduction of the acetylene groups, the long branched C32 alkyl chain means that it has high solubility; it is soluble in the solvents chloroform, chlorobenzene, and dichlorobenzene at concentrations of 10 mg mL^{-1}.

The thermal properties of PDPP-TAT were characterized by performing thermogravimetric analysis (TGA) and differential scanning calorimetry (DSC). A weight loss of 5% was observed at 393 °C, and a sharp endothermic peak occurred at 250 °C during heating. These results imply that PD PP-TAT has good thermal endurance and is crystalline (see the Supporting Information). Table 1 summarizes the electrochemical and optical absorption properties of PDPP-TVT and PDPP-TAT.

Table 1. Energy Levels of PDPP-TVT and PDPP-TAT: Optical Bandgap (E_g), LUMO Levels (E_{LUMO}), and HOMO Levels (E_{HOMO}) As Derived from the UV−vis Absorption Spectra and Cyclic Voltammetry Curves

UV−vis peak (nm)	E_g (eV)	E_{LUMO} (eV)	E_{HOMO} (eV)
PDPP-TVT			
780[a] 796, 721[b]	1.22	4.15	5.37
PDPP-TAT			
761[a] 765, 692[b]	1.50	3.89	5.39

[a]Solution samples. [b]Thermally annealed thin films.

According to the UV−vis absorption spectra in Figure 1, PDPP-TVT and PDPP-TAT thin films have optical band gaps of 1.22 and 1.50 eV, respectively, which were calculated from the onset absorptions of thin films of the polymers. The HOMO levels of PDPP-TVT and PDPP-TAT estimated from cyclic voltammograms were 5.37 and 5.39 eV, respectively. PDPP-TAT with its *sp*-hybridized acetylene linkages has a slightly deeper HOMO level than PDPP-TVT with sp^2-hybridized vinylene linkages[38−41] because of the electron-withdrawing nature of the acetylene linkages. However, the absorption of PDPP-TAT is blue-shifted, relative to that of PDPP-TVT, which implies that the "push−pull" effect between donor and acceptor moieties is somewhat disrupted by the acetylene linkages.[40,41]

It seems possible from these considerations that the acetylene linkages could negatively impact the intramolecular charge transfer between tDPP and TAT. However, the actual charge transport properties are quite different. Top-contact and bottom-gate FETs were fabricated. To enable favorable electron injection and achieve ambipolar FETs, aluminum was used for the source-drain electrodes instead of gold. Cytop-coated SiO_2 with a capacitance of 8.1 nF cm^{-2} was used as the

dx.doi.org/10.1021/cm5014703 | *Chem. Mater.* XXXX, XXX, XXX−XXX

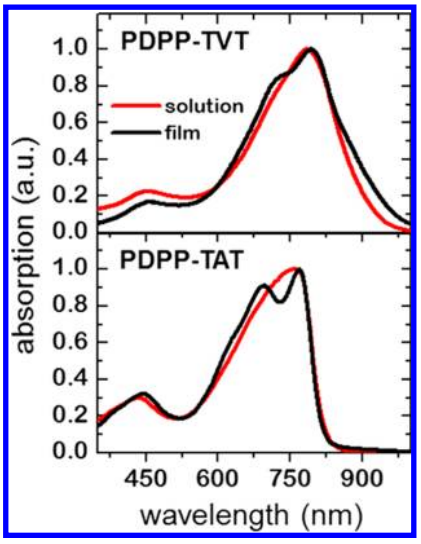

Figure 1. Normalized UV-absorption spectra of (top) PDPP-TVT and (bottom) PDPP-TAT.

gate dielectric. Cytop is a well-known material that forms defect-free surfaces, so Cytop-based FETs are expected to exhibit the near-intrinsic electrical properties of the synthesized polymers.[42−45] Figure 2a shows transfer characteristic curves (drain current I_D − gate voltage V_G with a fixed drain voltage V_D) of the PDPP-TVT and PDPP-TAT FETs. To investigate ambipolar charge transport in these FETs, both *p*-mode (V_G, V_D < 0, red squares) and *n*-mode (V_G, V_D > 0, blue circles) sweeps were performed in the saturation region. The curve shapes and on-current levels indicate that the PDPP-TAT FETs produce ambipolar V-shaped transfer curves, in contrast to the PDPP-TVT FETs, which produce unipolar L-shaped transfer curves. The hole (μ_h) and electron (μ_e) FET mobilities were obtained by using the following equation for the saturation regime:

$$I_D = \frac{W}{2L} C_i \mu_{h\,or\,e} (V_G - V_{th})^2 \quad (1)$$

where W/L is the channel width/length, C_i is the capacitance of the Cytop/SiO_2 gate-dielectric, and V_{th} is the threshold voltage. The FET mobilities were calculated from the slopes in the $|I_D|^{1/2} - V_G$ curves (the black lines in Figure 2a). Figure 2b and Table 2 show the hole and electron mobilities of the devices for various thermal annealing (TA) temperatures. The PDPP-TVT FETs exhibit high μ_h values with a maximum value of 5.10 cm^2 V^{-1} s^{-1}, which is consistent with the results of Kang et al.[34] and Chen et al.[28] PDPP-TVT FETs also exhibit electron channel accumulation, but μ_e (0.02 cm^2 V^{-1} s^{-1}) is much lower than μ_h. The PDPP-TAT FETs exhibit μ_h values that are 2−2.5 times lower than those of the PDPP-TVT FETs with a maximum value of 2.19 cm^2 V^{-1} s^{-1}, which is consistent with our expectation from the UV−vis spectrum. However, the PDPP-TAT devices exhibit μ_e values that are 15 times higher than those of the PDPP-TVT FETs, with a maximum value of 0.38 cm^2 V^{-1} s^{-1}. As a result, the μ_e/μ_h ratios shown in Figure 2c are low for the PDPP-TVT FETs (∼0.008), whereas those of the PDPP-TAT FETs are almost 30 times higher (∼0.26), which means that the PDPP-TAT FETs are possible to form both hole- and electron-accumulated channels with high mobilities, in contrast to the PDPP-TVT FETs. The output curves of the PDPP-TAT FETs (I_D − V_D, with a V_G step (see

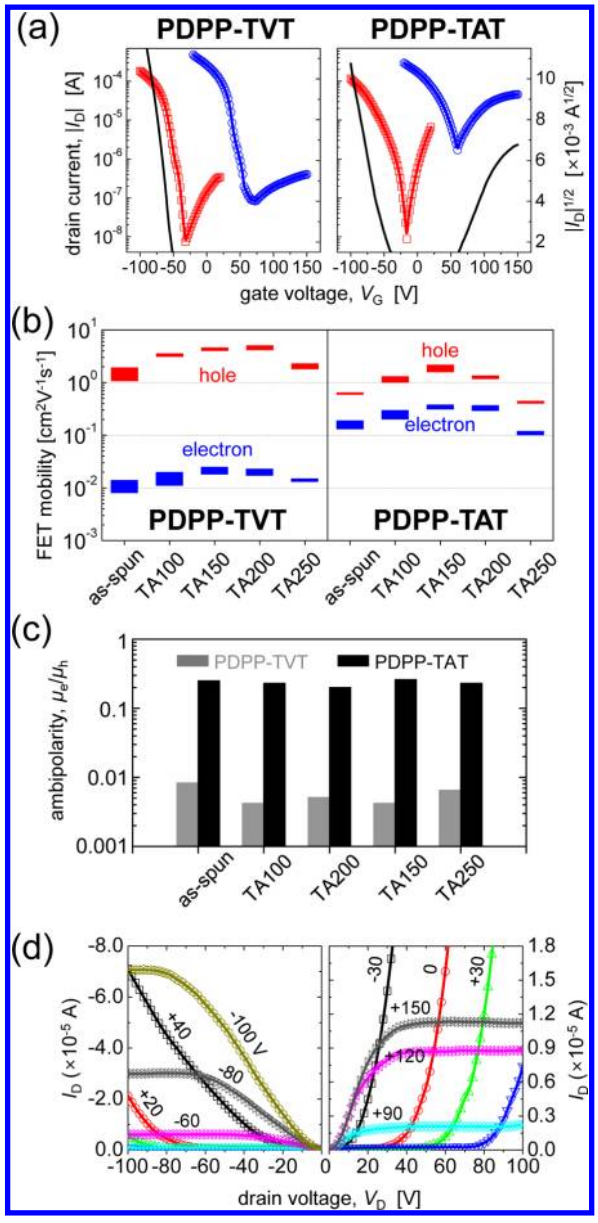

Figure 2. (a) Transfer characteristic (I_D−V_G) curves of (left) PDPP-TVT and (right) PDPP-TAT FETs. The polymer thin films were annealed at 150 °C for 10 min. *p*-mode sweeps (red square) and *n*-mode sweeps (blue circle) were performed at V_D= −100 and +100 V, respectively. The black solid lines are $|I_D|^{1/2}$−V_G curves whose slopes are proportional to the FET mobilities. (b) The range of electron and hole mobilities of (left) PDPP-TVT and PDPP-TAT (right) FETs according to the thermal annealing (TA) temperature (100, 150, 200, and 250 °C). (c) The average electron/hole mobility ratio (μ_e/μ_h) of PDPP-TVT (gray) and PDPP-TAT (black) FETs. (d) Output characteristic (I_D−V_D) curves of PDPP-TAT FETs.

Figure 2d)) are typical of ambipolar FETs. Both polymer FETs exhibited almost hysteresis-free curves in *p*-mode sweep, whereas they exhibited noticeable hysteresis in *n*-mode sweep (see Figure S13 in the Supporting Information). Furthermore, the PDPP-TVT FETs exhibited a rather wider hysteresis gap in *n*-mode sweep than the PDPP-TAT FETs. These results indicate that both PDPP-TVT and PDPP-TAT FETs contain several electron trap sites, which are considered to hinder the formation of electron-accumulated channel and increase the threshold voltages in *n*-mode sweep. However, from the result

dx.doi.org/10.1021/cm5014703 | *Chem. Mater.* XXXX, XXX, XXX−XXX

Table 2. Field-Effect Electron and Hole Mobilities (μ_e and μ_h, Respectively) of PDPP-TVT (up) and PDPP-TAT (down) FETs for Various Thermal Annealing (TA) Temperatures[a]

	Electron Mobility, μ_e ($cm^2\ V^{-1}\ s^{-1}$)		Hole Mobility, μ_h ($cm^2\ V^{-1}\ s^{-1}$)		
	(average)	(max)	(average)	(max)	μ_e/μ_h
PDPP-TVT					
as-spun	0.009	0.014	1.09	1.94	8.3×10^{-3}
TA100	0.014	0.020	3.30	3.59	4.2×10^{-3}
TA150	0.021	0.025	4.05	4.64	5.1×10^{-3}
TA200	0.018	0.023	4.31	5.10	4.2×10^{-3}
TA250	0.014	0.015	1.95	2.31	6.5×10^{-3}
PDPP-TAT					
as-spun	0.15	0.19	0.61	0.65	2.5×10^{-1}
TA100	0.25	0.30	1.10	1.32	2.3×10^{-1}
TA150	0.33	0.38	1.71	2.19	2.0×10^{-1}
TA200	0.31	0.37	1.21	1.36	2.6×10^{-1}
TA250	0.10	0.12	0.44	0.45	2.3×10^{-1}

[a]The ambipolarities (μ_e/μ_h) are calculated from the average values.

of hysteresis gap, the PDPP-TAT FETs are considered to contain less electron trap sites than the PDPP-TVT FETs.

To investigate the molecular ordering of the polymer thin films, we compared their two-dimensional grazing incident X-ray diffraction (2D-GIXD) patterns (see Figure 3). In the out-of-plane patterns of both thin films, (h00) diffraction peaks are dominant. The observed interlayer distances of (h00) are much shorter than that of the fully extended alkyl side chains, and are similar to each other, even though the alkyl chain lengths are rather different: $d_{(h00)}$ = 21.2 Å for PDPP-TVT and 21.0 Å for PDPP-TAT, as calculated from their (100) peaks at q_z = 2.96 and 3.00 nm^{-1}. This similarity might be due to the interdigitation of the alkyl side chains. A side chain on one of these polymers can easily interdigitate with the side chains of an adjacent polymer, because of the lack of aliphatic side groups in the donor components. Moreover, this interdigitation does not hinder the coplanarity of the main chain. The (010) diffraction peaks are present at q_{xy} = 16.82 and 17.36 nm^{-1} for PDPP-TVT and PDPP-TAT, respectively, so the $\pi-\pi$ stacking distances are 3.74 Å for PDPP-TVT and 3.62 Å for PDPP-TAT. These values are quite small and can only be achieved when the co-planarity of the main chain is preserved. This co-planarity is one advantage of tDPP-based co-polymer systems with rigid linkages. Furthermore, the smaller characteristic distance of PDPP-TAT in both the (100) and (010) planes is thought to originate from the cylinder-like forms of the rich π-electrons in the acetylene linkages. Each carbon atom in the acetylene linkages contains an additional p-orbital, which is perpendicular to the other p-orbital. We speculate that not only do these additional p-orbitals enrich π-electrons in the acetylene linkages, enhancing the $\pi-\pi$ interactions along [010], but their direction also assists attracting neighbor molecules located on [100]. For both the PDPP-TVT and PDPP-TAT thin films, the diffraction peaks (h00) and (0k0) are predominantly observed along the out-of-plane and in-plane, respectively, which indicates that the polymers have predominantly edge-on orientations, with respect to the substrate.[46] The intensities of both peaks increase and become saturated with increases in the annealing temperature, which is consistent with the variations in μ_h and μ_e. From the height and phase profiles obtained with atomic force microscopy (AFM), needlelike features, which are

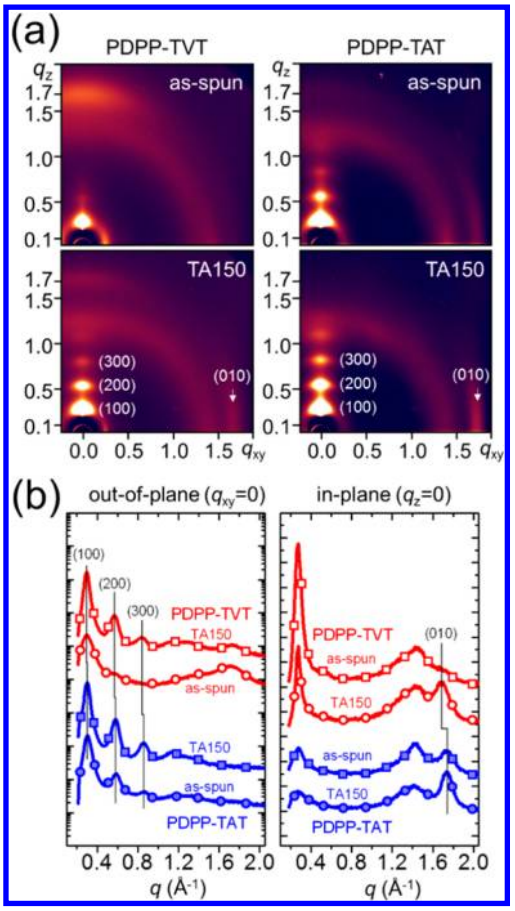

Figure 3. (a) Two-dimensional grazing-incidence X-ray diffraction (2D-GIXD) patterns of PDPP-TVT (left) and PDPP-TAT (right) thin films. TA150 is a film post-annealed at 150 °C for 15 min. (b) Out-of-plane (left) and in-plane (right) X-ray diffraction patterns of PDPP-TVT (red) and PDPP-TAT (blue) thin films. The profiles were obtained from the 2D-GIXD patterns. (100), (200), and (300) correspond to molecular stacking in the direction of the alkyl side chain, and (010) corresponds to $\pi-\pi$ stacking of the main chain.

thought to be PDPP-TAT crystalline domains, are present in the as-spun films and in those annealed at 100 and 150 °C, but start to disappear above 200 °C (see Figures 4a–c). The 2D-GIXD and AFM results and the FET mobilities suggest that there is a strong correlation between the crystallinity and the FET mobilities.[47−49]

In general, several factors determine FET performances, such as molecular weight, process conditions, morphology, and crystallinity. In this research, we tried to synthesize similar molecular weights and use the same fabrication processes in comparing PDPP-TAT with PDPP-TVT. Besides, both polymer thin films exhibit similar morphologies with needle-like features, have similar d-spacing of (100) and (010), and exhibit the same edge-on dominant structures. However, PDPP-TAT has slightly longer side chains than PDPP-TVT, and another quantitative information about crystallinity such as portion and size of crystalline phases can be slightly different. These might be the origin of the 2–2.5 times lower hole mobility of PDPP-TAT FETs, but they are not sufficient for our discussion of the remarkably different electron FET mobility and ambipolarity. Note that:

(1) TT[tDPP]-structured co-polymers typically only exhibit p-type FET characteristics,[25,28,29,34,35]

dx.doi.org/10.1021/cm5014703 | Chem. Mater. XXXX, XXX, XXX−XXX

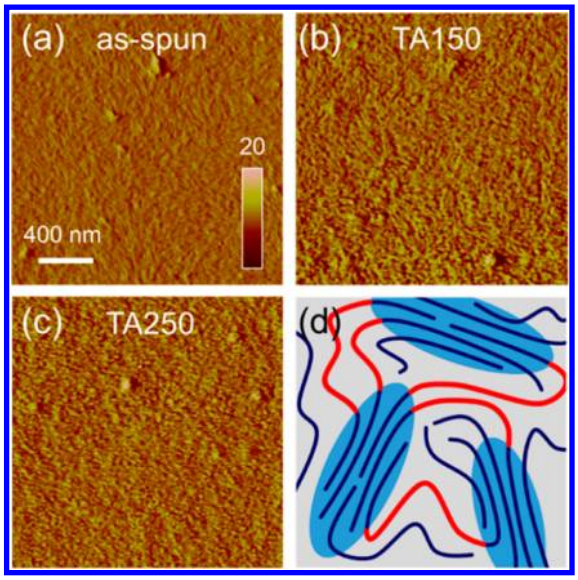

Figure 4. AFM phase images of PDPP-TAT films: (a) as-spun thin film, (b) TA150, and (c) TA250. TA150 and TA250 are the films post-annealed at 150 and 250 °C for 15 min, respectively. (d) Schematic diagram of the complex microstructure of the PDPP-TAT thin film, which consists of needle-shaped crystalline domains and disordered amorphous regions. Tie-molecules connecting crystalline domains are highlighted in red. The molecular orientations of the crystalline domains do not exactly correspond to those in the diagram.

(2) the π-conjugation length of PDPP-TAT is likely to be a little shorter than that of PDPP-TVT according to the UV−vis spectra, and, most importantly,
(3) localization/delocalization of electron wave functions also has crucial influence on electron transport.[21,50]

It is likely that the origin of the ambipolarity lies on the molecular level. Several papers have explained the ambipolarity of synthesized polymers in terms of the delocalized charge-density isosurfaces of both their highest occupied molecular orbital (HOMO) and lowest unoccupied molecular orbital (LUMO) levels.[51−53] Hence, computational calculations using density-functional theory (DFT, B3LYP/6-31G) have been performed.[54] A comparison of the distributions of the electron wave functions near the vinylene and acetylene linkages is vital to this discussion, so we constructed a model of the "tDPP−donor−tDPP" system. Since the side alkyl chains do not contribute significantly to the variations in the charge-density isosurface, they were replaced by methyl groups in our calculations. Energy optimizations were performed for PDPP-TVT and PDPP-TAT.

Figure 5 shows the DFT-calculated charge density isosurfaces for the HOMO and LUMO levels of the two molecules. These results show that co-planarity is favored for PDPP-TVT and PDPP-TAT. These co-planar forms are likely to facilitate intermolecular $\pi-\pi$ interactions and the formation of crystalline domains. The crystalline peaks in the 2D-GIXD patterns and the needlelike crystalline domains probably originate from the stacking of the optimized co-planar molecules. However, the distributions of charge density in the HOMO and LUMO levels cannot explain their very different ambipolarities (μ_e/μ_h) in FETs; the charge densities of the HOMO and LUMO levels of both PDPP-TAT and PDPP-TVT are delocalized over the entire conjugated backbones in the co-planar state.

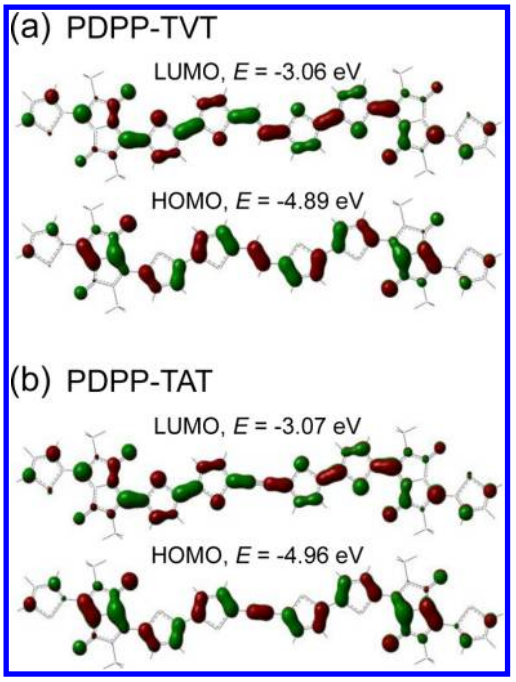

Figure 5. DFT-optimized geometries and charge-density isosurfaces for the LUMO and HOMO levels of (a) PDPP-TVT and (b) PDPP-TAT (B3LYP/6-31G, isovalue = 0.028). The optimized geometries of both polymers are almost co-planar.

Thus, the results of our calculations suggest that both PDPP-TVT and PDPP-TAT can be used to produce ambipolar FETs. However, this conclusion assumes the presence of the optimized co-planar state. Even though needlelike network morphologies were observed in both PDPP-TAT and PDPP-TVT films,[28] conjugated polymer chains such as PDPP-TVT and PDPP-TAT inevitably have amorphous phases and tie molecules with many degrees of conformational freedom, which results in complex microstructures in the solid state (Figure 4d). The amorphous hollows in the 2D-GIXD patterns (Figure 3a) also indicate the presence of polymeric chains in various conformations. Very recently, Salleo and Podzorov emphasized the importance of polymeric chains that connect crystalline domains.[55−57] Even though the co-planar forms of PDPP-TVT and PDPP-TAT are energetically favorable, small twists of the PDPP-TVT and PDPP-TAT monomer units are also energetically possible via thermal energy (see Figure S14 in the Supporting Imformation), and tie molecules cannot maintain the co-planar state in order to connect crystalline domains.

Hence, it is possible that some polymeric chains are present in a tie-molecular phase (as a result of changes in chain conformation), so we investigated in detail the charge density isosurfaces of the HOMO and LUMO levels. Figures 6 and 7 show the charge density isosurfaces for the HOMO/LUMO levels of PDPP-TVT and PDPP-TAT, respectively, as functions of the dihedral angle. The vinylene and acetylene linkages are considered to be the key positions determining ambipolarity, so we focused on the thiophene−vinylene (T-V) and thiophene−acetylene (T-A) bonds; the dihedral angles ($\phi_{T\text{-}V}$ for PDPP-TVT and $\phi_{T\text{-}A}$ for PDPP-TAT) were varied from the co-planar state ($\phi = 0°$), as shown in Figures 6a and 7a). Interestingly, we found that the π-conjugation of PDPP-TVT is sensitive to the chain twist (Figure 6b), whereas that of PDPP-TAT is highly insensitive (Figure 7b) to the chain twist. In the case of PDPP-

dx.doi.org/10.1021/cm5014703 | Chem. Mater. XXXX, XXX, XXX−XXX

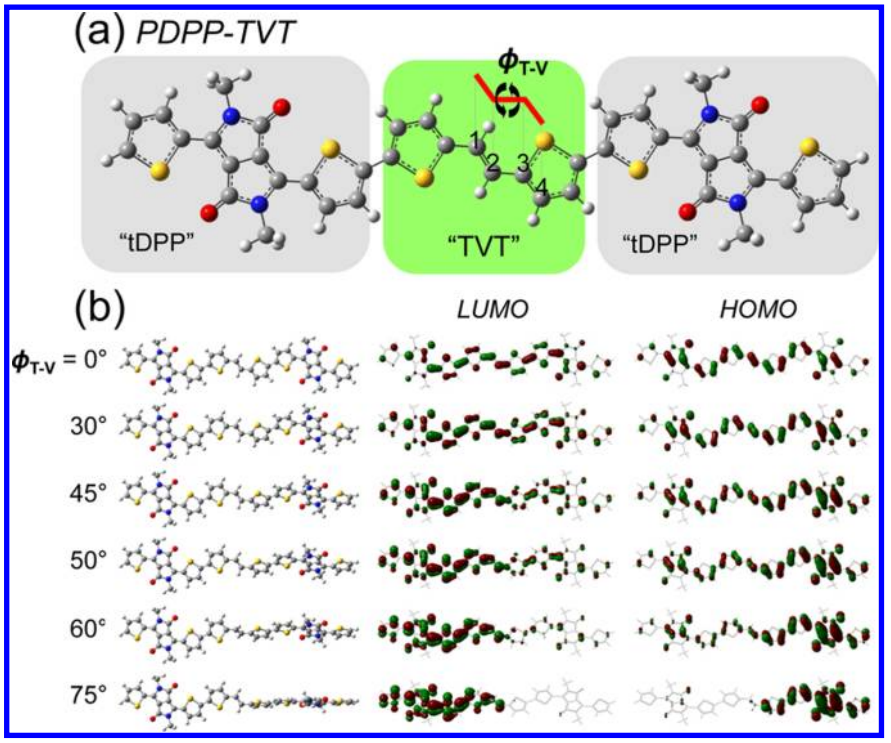

Figure 6. (a) Molecular structure of PDPP-TVT model system and the definition of dihedral angle ϕ at the C_{1234} carbon group. The twist occurs at thiophene−vinylene (T-V) bond. (b) Views of spirally twisted tDPP−TVT−tDPP at twist angles (ϕ) of 0°−75° (left). DFT-calculated charge-density isosurfaces for the LUMO (middle) and HOMO (right) levels as a function of ϕ (B3LYP/6-31G, isovalue = 0.028). ϕ = 0° is the co-planar state.

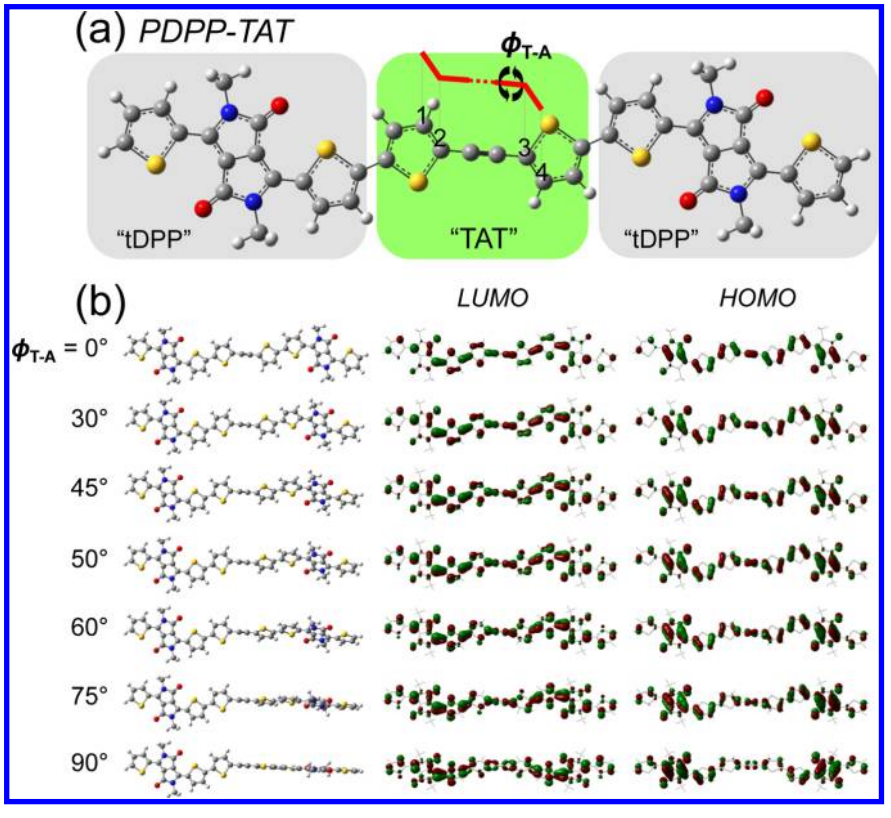

Figure 7. (a) Molecular structure of PDPP-TAT model system and the definition of dihedral angle ϕ at the C_{1234} carbon group. The twist was performed at thiophene−acetylene (T-A) bond. (b) Views of spirally twisted tDPP−TAT−tDPP at twist angles(ϕ) of 0−90° (left). DFT-calculated charge-density isosurfaces for the LUMO (middle) and HOMO (right) levels as a function of ϕ (B3LYP/6-31G, isovalue = 0.028). ϕ = 0° is the co-planar state.

dx.doi.org/10.1021/cm5014703 | *Chem. Mater.* XXXX, XXX, XXX−XXX

TVT, the well-distributed LUMO and HOMO isosurfaces become monotonically localized when $\phi_{T\text{-}V}$ is in the range of 0°−60° (Figure 6b), which indicates that charge transfer in the LUMO and HOMO states is interrupted by the twisting of the T-V bonds. In particular, note that the charge transfer at the LUMO is more prone to be interrupted than that at the HOMO; the delocalization of the LUMO is more sensitive to the dihedral angle ϕ than that of the HOMO (see LUMO/HOMO at $\phi_{T\text{-}V}$ = 45°−60°). This difference arises because the bonding interactions of the LUMO are located on the T-T and V-T bonds and those of the HOMO are located within T and V (see Figure 5).[1,58] Thus, hole transport along the intrachain is more insensitive to the chain twist than electron transport. In the case of PDPP-TAT, however, the well-distributed LUMO and HOMO isosurfaces are maintained, even at high $\phi_{T\text{-}A}$ (Figure 7b). Thus, the π-conjugation and charge transfer at the LUMO and HOMO states are highly insensitive to the twisting of the T-A bonds. This remarkable difference between PDPP-TVT and PDPP-TAT explains the differences between the electron transport in their actual FET devices. In the amorphous and tie-molecular regions within the actual thin films, the T-V bonds in PDPP-TVT and T-A bonds in PDPP-TAT are twisted by changes in chain conformation. In the case of PDPP-TVT, the electron transport between the crystalline domains along twisted chains is interrupted by diminished π-conjugation. However, for PDPP-TAT, twisting around the acetylene linkages does not diminish the π-conjugation, which means that the PDPP-TAT FETs exhibit μ_e values 15 times higher than those of the PDPP-TVT FETs.

The twist-insensitive π-conjugation of PDPP-TAT originates from the *sp*-hybridized carbon atoms in the acetylene linkages. Figures 8a and 8b show the *p*-orbitals of the carbon atoms in PDPP-TVT and PDPP-TAT when $\phi \neq 0°$. The twists were performed between the A carbon atom (in thiophene) and the B carbon atom (in the vinylene or acetylene linkages). In PDPP-TVT, $p_{z(A)}$ is not present on the same plane as $p_{z(B)}$, because of the twisting; hence, the interaction $p_{z(A)}$−$p_{z(B)}$ becomes monotonically weakened with increases in $\phi_{T\text{-}V}$. However, in PDPP-TAT, each carbon atom in the acetylene linkage has one more *p*-orbital ($p_{y(B)}$), so the $p_{z(A)}$−$p_{y(B)}$ interaction increases with $\phi_{T\text{-}A}$. This combination of $p_{z(A)}$−$p_{z(B)}$ and $p_{z(A)}$−$p_{y(B)}$ interactions means that the π−π interactions are sustained, regardless of variation in the ϕ of PDPP-TAT.

Actually, high twist angles such as ϕ = 45°−90° are not energetically possible. Under these low twist angles of the T−V bonds in PDPP-TVT, the HOMO and LUMO isosurfaces can maintain their delocalization in a monomer unit, but the delocalization of the LUMO must be more weakened than that of the HOMO. This difference will be noticeably increased as the number of the twisted monomer unit increases. Because a large twist of a polymeric chain in tie-molecular regions can arise as the sum of the small twists of the monomer units, the LUMO isosurfaces in tie-molecular regions lose their delocalization in, whereas the HOMO isosurfaces can still maintain their delocalization. It results in unfavorable electron transport between the crystalline domains and low values of μ_e and μ_e/μ_h for the PDPP-TVT FETs. In contrast, twists of the T−A bonds do not significantly affect the intrachain electron transport, and, thus, the electron transport between crystalline domains is much more favorable in PDPP-TAT, with high values of μ_e and μ_e/μ_h. Even though further in-depth analysis and study are required, we suggest that the differences between

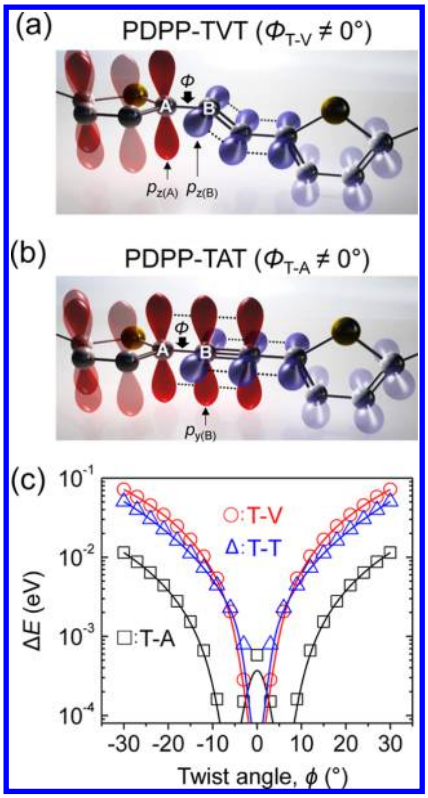

Figure 8. *p*-orbitals of the carbon atoms in (a) PDPP-TVT and (b) PDPP-TAT when $\phi \neq 0°$. The carbon atom in the vinylene linkage contains only a p_z-orbital, whereas that in acetylene linkage has an additional p_y-orbital. (c) The shifts in the internal potential energy (ΔE) of PDPP-TVT and PDPP-TAT as functions of the twist angles (ϕ) of thiophene−vinylene (T−V), thiophene−acetylene (T−A), and thiophene−thiophene (T-T). The twisting of the T−V and T−T bonds is performed to PDPP-TVT and that of T−A bond is performed to PDPP-TAT.

the variations in the internal energy shifts as a function of ϕ of the two co-polymers mean that the electron transport properties of their amorphous and tie-molecular phases are different. In PDPP-TVT and PDPP-TAT, most changes in chain conformation arise as a result of twists of the T−T, T−V, and T−A bonds. The T−T bond has a π-conjugation structure that is similar to that of the T−V bond, so the π-conjugation of the T−T bond is also rather unstable, with respect to twisting. As shown in Figure 8c, twists of the T−T and T−V bonds are energetically similar and the twist of the T−A bond is energetically the most favorable. Based on these results, we suggest that in PDPP-TVT both T−T and T−V bonds twist for the conformational changes of the polymer backbones, and intrachain electron transport is gradually interrupted at these sites. In the case of PDPP-TAT, however, most changes in conformation arise through the twists of T−A bonds and slight twists of T−T bonds. As a result, the reductions in electron transport along the T−T bonds of PDPP-TAT in the amorphous and tie-molecular phases are less upon changes in conformation.

The presence of ambipolarity in the PDPP-TAT FETs prompted us to investigate the properties of CMOS-like inverters consisting of two identical ambipolar FETs with a common gate as the input voltage (V_{in}) (Figure 9a). Figures 9b and 9c show the output voltage (V_{out}) as a function of the input voltage (V_{in}) at a constant supply bias (V_{DD}). The slopes of the

dx.doi.org/10.1021/cm5014703 | *Chem. Mater.* XXXX, XXX, XXX−XXX

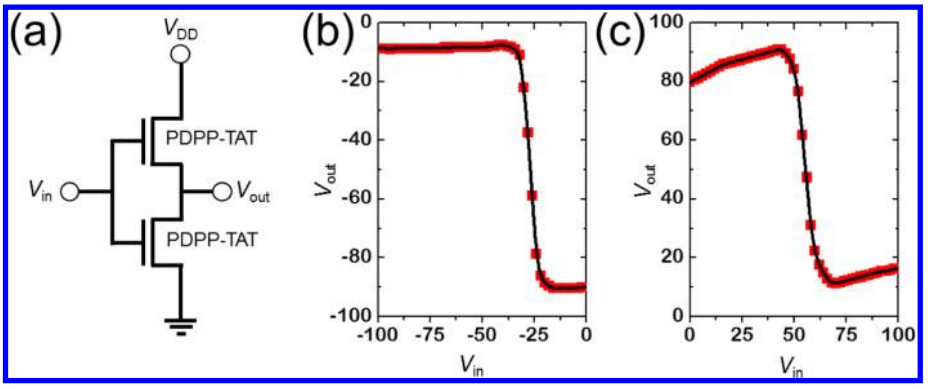

Figure 9. (a) Circuit diagram of the complementary inverter structure based on two identical PDPP-TAT FETs. (b, c) CMOS-like inverter characteristics of the inverter.

inverter curve indicate maximum gains of ~10 for the *p*-mode and ~7 for the *n*-mode. The *n*-mode exhibits smaller gain and more unstable operation, which might originate from electron charge trapping during operation, the origin of which remains to be explained.

CONCLUSION

In summary, we have demonstrated that a tDPP-based co-polymer with a TT[tDPP] structure can exhibit ambipolarity. The synthesized co-polymer PDPP-TAT contains acetylene linkages within the donor components, which are more electron-withdrawing than vinylene or ethane linkages. Even though the push−pull effect of PDPP-TAT is somewhat weaker than that of PDPP-TVT, the intrachain electron transport of PDPP-TAT is much more insensitive to the chain conformation than that of PDPP-TVT. As a result, PDPP-TAT exhibits much more favorable electron transport in its amorphous and tie-molecular phases and its FET devices exhibit a high electron mobility (0.38 $cm^2\ V^{-1}\ s^{-1}$) and a high hole mobility (2.19 $cm^2\ V^{-1}\ s^{-1}$), as well as an ambipolarity (μ_e/μ_h = 0.26) that is 30 times higher than that of PDPP-TVT. Our research demonstrates the potential of acetylene linkages for high-performance ambipolar FETs based on D−A co-polymers. Furthermore, the conformation-insensitive charge transport is considered as an important factor in the electrical performances of actual devices.

ASSOCIATED CONTENT

Supporting Information

Complete synthetic procedure and characterization of all the intermediates (NMR, DSC, TGA, and Cyclic voltammograms), AFM morphologies and 2D-GIXD patterns of the thin films according to the postannealing temperature, transfer characteristic curves according to the thermal annealing temperatures, and DFT calculations.This material is available free of charge via the Internet at http://pubs.acs.org.

AUTHOR INFORMATION

Corresponding Authors

*E-mail: skwon@gnu.ac.kr (S.-K. Kwon).
*E-mail: ykim@gnu.ac.kr (Y.-H. Kim).
*E-mail: kwcho@postech.ac.kr (K. Cho).

Author Contributions

$^{\nabla}$These authors contributed equally.

Notes

The authors declare no competing financial interest.

ACKNOWLEDGMENTS

This work was supported by a grant (Code No.2011-0031628) from the Center for Advanced Soft Electronics under the Global Frontier Research Program of the Ministry of Science, ICT & Future Planning, Korea.

ABBREVIATIONS

DPP, diketopyrrolopyrrole
tDPP, dithienyl-diketopyrrolopyrrole
T, thiophene
S, selenophene
V and =, vinylene linkage
A and ≡, acetylene linkage
T-V, single bond between thiophene and vinylene linkage
T-A, single bond between thiophene and acetylene linkage
T-T, single bond between thiophenes

REFERENCES

(1) Bao, Z.; Locklin, J. J. *Organic Field-Effect Transistors*; CRC Press: Boca Raton, FL, 2007.
(2) Kang, B.; Lee, W. H.; Cho, K. *ACS Appl. Mater. Interfaces* **2013**, *5*, 2302.
(3) Meijer, E. J.; de Leeuw, D. M.; Setayesh, S.; van Veenendaal, E.; Huisman, B. H.; Blom, P. W. M.; Hummelen, J. C.; Scherf, U.; Klapwijk, T. M. *Nat. Mater.* **2003**, *2*, 678.
(4) Crone, B.; Dodabalapur, A.; Lin, Y. Y.; Filas, R. W.; Bao, Z.; LaDuca, A.; Sarpeshkar, R.; Katz, H. E.; Li, W. *Nature* **2000**, *403*, 521.
(5) Zaumseil, J.; Sirringhaus, H. *Chem. Rev.* **2007**, *107*, 1296.
(6) Lee, W. H.; Cho, J. H.; Cho, K. *J. Mater. Chem.* **2010**, *20*, 2549.
(7) Bürgi, L.; Turbiez, M.; Pfeiffer, R.; Bienewald, F.; Kirner, H.-J.; Winnewisser, C. *Adv. Mater.* **2008**, *20*, 2217.
(8) McCulloch, I.; Heeney, M.; Bailey, C.; Genevicius, K.; MacDonald, I.; Shkunov, M.; Sparrowe, D.; Tierney, S.; Wagner, R.; Zhang, W.; Chabinyc, M. L.; Kline, R. J.; McGehee, M. D.; Toney, M. F. *Nat. Mater.* **2006**, *5*, 328.
(9) Sirringhaus, H.; Brown, P. J.; Friend, R. H.; Nielsen, M. M.; Bechgaard, K.; Langeveld-Voss, B. M. W.; Spiering, A. J. H.; Janssen, R. A. J.; Meijer, E. W.; Herwig, P.; de Leeuw, D. M. *Nature* **1999**, *401*, 685.
(10) Rost, C.; Gundlach, D. J.; Karg, S.; Riess, W. *J. Appl. Phys.* **2004**, *95*, 5782.
(11) Yoon, M.-H.; Kim, C.; Facchetti, A.; Marks, T. J. *J. Am. Chem. Soc.* **2006**, *128*, 12851.
(12) Kunugi, Y.; Takimiya, K.; Negishi, N.; Otsubo, T.; Aso, Y. *J. Mater. Chem.* **2004**, *14*, 2840.
(13) Usta, H.; Risko, C.; Wang, Z.; Huang, H.; Deliomeroglu, M. K.; Zhukhovitskiy, A.; Facchetti, A.; Marks, T. J. *J. Am. Chem. Soc.* **2009**, *131*, 5586.

(14) Takahashi, T.; Takenobu, T.; Takeya, J.; Iwasa, Y. *Appl. Phys. Lett.* **2006**, *88*, 033505.
(15) Chesterfield, R. J.; Newman, C. R.; Pappenfus, T. M.; Ewbank, P. C.; Haukaas, M. H.; Mann, K. R.; Miller, L. L.; Frisbie, C. D. *Adv. Mater.* **2003**, *15*, 1278.
(16) Facchetti, A. *Chem. Mater.* **2010**, *23*, 733.
(17) Wang, C. L.; Dong, H. L.; Hu, W. P.; Liu, Y. Q.; Zhu, D. B. *Chem. Rev.* **2012**, *112*, 2208.
(18) Zhao, Y.; Guo, Y.; Liu, Y. *Adv. Mater.* **2013**, *25*, 5372.
(19) Lee, W.-Y.; Giri, G.; Diao, Y.; Tassone, C. J.; Matthews, J. R.; Sorensen, M. L.; Mannsfeld, S. C. B.; Chen, W.-C.; Fong, H. H.; Tok, J. B. H.; Toney, M. F.; He, M.; Bao, Z. *Adv. Funct. Mater.* **2014**, *24*, 3524.
(20) Liu, F.; Wang, C.; Baral, J. K.; Zhang, L.; Watkins, J. J.; Briseno, A. L.; Russell, T. P. *J. Am. Chem. Soc.* **2013**, *135*, 19248.
(21) Nielsen, C. B.; Turbiez, M.; McCulloch, I. *Adv. Mater.* **2013**, *25*, 1859.
(22) Li, Y. N.; Sonar, P.; Murphy, L.; Hong, W. *Energy Environ. Sci.* **2013**, *6*, 1684.
(23) Zoombelt, A. P.; Mathijssen, S. G. J.; Turbiez, M. G. R.; Wienk, M. M.; Janssen, R. A. J. *J. Mater. Chem.* **2010**, *20*, 2240.
(24) Li, Y.; Sun, B.; Sonar, P.; Singh, S. P. *Org. Electron.* **2012**, *13*, 1606.
(25) Kang, I.; Yun, H. J.; Chung, D. S.; Kwon, S. K.; Kim, Y. H. *J. Am. Chem. Soc.* **2013**, *135*, 14896.
(26) Lei, T.; Dou, J. H.; Pei, J. *Adv. Mater.* **2012**, *24*, 6457.
(27) Lee, J. S.; Son, S. K.; Song, S.; Kim, H.; Lee, D. R.; Kim, K.; Ko, M. J.; Choi, D. H.; Kim, B.; Cho, J. H. *Chem. Mater.* **2012**, *24*, 1316.
(28) Chen, H.; Guo, Y.; Yu, G.; Zhao, Y.; Zhang, J.; Gao, D.; Liu, H.; Liu, Y. *Adv. Mater.* **2012**, *24*, 4618.
(29) Li, Y.; Sonar, P.; Singh, S. P.; Soh, M. S.; van Meurs, M.; Tan, J. *J. Am. Chem. Soc.* **2011**, *133*, 2198.
(30) Bijleveld, J. C.; Zoombelt, A. P.; Mathijssen, S. G. J.; Wienk, M. M.; Turbiez, M.; de Leeuw, D. M.; Janssen, R. A. J. *J. Am. Chem. Soc.* **2009**, *131*, 16616.
(31) Zhang, X.; Richter, L. J.; DeLongchamp, D. M.; Kline, R. J.; Hammond, M. R.; McCulloch, I.; Heeney, M.; Ashraf, R. S.; Smith, J. N.; Anthopoulos, T. D.; Schroeder, B.; Geerts, Y. H.; Fischer, D. A.; Toney, M. F. *J. Am. Chem. Soc.* **2011**, *133*, 15073.
(32) Lin, H.-W.; Lee, W.-Y.; Chen, W.-C. *J. Mater. Chem.* **2012**, *22*, 2120.
(33) Lee, W.-H.; Son, S. K.; Kim, K.; Lee, S. K.; Shin, W. S.; Moon, S.-J.; Kang, I.-N. *Macromolecules* **2012**, *45*, 1303.
(34) Kang, I.; An, T. K.; Hong, J.-a.; Yun, H.-J.; Kim, R.; Chung, D. S.; Park, C. E.; Kim, Y.-H.; Kwon, S.-K. *Adv. Mater.* **2013**, *25*, 524.
(35) Tsai, J.-H.; Lee, W.-Y.; Chen, W.-C.; Yu, C.-Y.; Hwang, G.-W.; Ting, C. *Chem. Mater.* **2010**, *22*, 3290.
(36) Li, J.; Zhao, Y.; Tan, H. S.; Guo, Y. L.; Di, C. A.; Yu, G.; Liu, Y. Q.; Lin, M.; Lim, S. H.; Zhou, Y. H.; Su, H. B.; Ong, B. S. *Sci. Rep. UK* **2012**, *2*, 754.
(37) Mio, M. J.; Kopel, L. C.; Braun, J. B.; Gadzikwa, T. L.; Hull, K. L.; Brisbois, R. G.; Markworth, C. J.; Grieco, P. A. *Org. Lett.* **2002**, *4*, 3199.
(38) Cremer, J.; Bäuerle, P.; Wienk, M. M.; Janssen, R. A. J. *Chem. Mater.* **2006**, *18*, 5832.
(39) Silvestri, F.; Marrocchi, A. *Int. J. Mol. Sci.* **2010**, *11*, 1471.
(40) Braunecker, W. A.; Oosterhout, S. D.; Owczarczyk, Z. R.; Larsen, R. E.; Larson, B. W.; Ginley, D. S.; Boltalina, O. V.; Strauss, S. H.; Kopidakis, N.; Olson, D. C. *Macromolecules* **2013**, *46*, 3367.
(41) Beaujuge, P. M.; Vasilyeva, S. V.; Ellinger, S.; McCarley, T. D.; Reynolds, J. R. *Macromolecules* **2009**, *42*, 3694.
(42) Sakanoue, T.; Sirringhaus, H. *Nat. Mater.* **2010**, *9*, 736.
(43) Minder, N. A.; Ono, S.; Chen, Z.; Facchetti, A.; Morpurgo, A. F. *Adv. Mater.* **2012**, *24*, 503.
(44) Kalb, W. L.; Mathis, T.; Haas, S.; Stassen, A. F.; Batlogg, B. *Appl. Phys. Lett.* **2007**, *90*, 092104.
(45) Yan, H.; Chen, Z.; Zheng, Y.; Newman, C.; Quinn, J. R.; Dötz, F.; Kastler, M.; Facchetti, A. *Nature* **2009**, *457*, 679.
(46) Kim, D. H.; Park, Y. D.; Jang, Y. S.; Yang, H. C.; Kim, Y. H.; Han, J. I.; Moon, D. G.; Park, S. J.; Chang, T. Y.; Chang, C. W.; Joo, M. K.; Ryu, C. Y.; Cho, K. W. *Adv. Funct. Mater.* **2005**, *15*, 77.
(47) Kwak, D.; Lim, J. A.; Kang, B.; Lee, W. H.; Cho, K. *Adv. Funct. Mater.* **2013**, *23*, 5224.
(48) Park, Y. D.; Kim, D. H.; Lim, J. A.; Cho, J. H.; Jang, Y.; Lee, W. R.; Park, J. H.; Cho, K. *J. Phys. Chem. C* **2008**, *112*, 1705.
(49) Lee, H. S.; Kim, D. H.; Cho, J. H.; Park, Y. D.; Kim, J. S.; Cho, K. *Adv. Funct. Mater.* **2006**, *16*, 1859.
(50) Shahid, M.; McCarthy-Ward, T.; Labram, J.; Rossbauer, S.; Domingo, E. B.; Watkins, S. E.; Stingelin, N.; Anthopoulos, T. D.; Heeney, M. *Chem. Sci.* **2012**, *3*, 181.
(51) Cho, S.; Lee, J.; Tong, M.; Seo, J. H.; Yang, C. *Adv. Funct. Mater.* **2011**, *21*, 1910.
(52) Lee, J.; Han, A. R.; Hong, J.; Seo, J. H.; Oh, J. H.; Yang, C. *Adv. Funct. Mater.* **2012**, *22*, 4128.
(53) Lee, J.; Han, A. R.; Kim, J.; Kim, Y.; Oh, J. H.; Yang, C. *J. Am. Chem. Soc.* **2012**, *134*, 20713.
(54) Ditchfield, R.; Hehre, W. J.; Pople, J. A. *J. Chem. Phys.* **1971**, *54*, 724.
(55) Podzorov, V. *Nat. Mater.* **2013**, *12*, 947.
(56) Noriega, R.; Rivnay, J.; Vandewal, K.; Koch, F. P. V.; Stingelin, N.; Smith, P.; Toney, M. F.; Salleo, A. *Nat. Mater.* **2013**, *12*, 1037.
(57) Noriega, R.; Salleo, A.; Spakowitz, A. J. *Proc. Natl. Acad. Sci. USA* **2013**, *110*, 16315.
(58) Zade, S. S.; Bendikov, M. *Chem.—Eur. J.* **2007**, *13*, 3688.